Eur. Phys. J. A **16**, 27–34 (2003)
DOI 10.1140/epja/i2002-10074-0

THE EUROPEAN PHYSICAL JOURNAL A

Antideuteron production in proton-proton and proton-nucleus collisions

R.P. Duperray[1,a], K.V. Protasov[1,b], and A.Yu. Voronin[2,c]

[1] Institut des Sciences Nucléaires, IN2P3-CNRS, UJFG, 53, Avenue des Martyrs, F-38026 Grenoble Cedex, France
[2] Lebedev Physical Institute, Leninsky prospekt, 53, 117924 Moscow, Russia

Received: 18 April 2002 / Revised version: 28 August 2002 /
Published online: 17 January 2003 –
Communicated by A. Molinari

Abstract. The experimental data of the antideuteron production in proton-proton and proton-nucleus collisions are analyzed within a simple model based on the diagrammatic approach to the coalescence model. This model is shown to be able to reproduce most of the existing data without any additional parameter.

PACS. 24.10.-i Nuclear-reaction models and methods

1 Introduction

The interest in the study of production of light antinuclei, in particular, antideuterons in proton-proton and proton-nucleus collisions has recently intensified. There are, at least, two major reasons for this. Firstly, studies of antideuteron production in cosmic space can be a very powerful tool to search for antimatter in the Universe [1]. It is planned to measure the antideuteron flux in the future AMS [2] and PAMELA [3] experiments.

Secondly, the possibility to make experiments with antideuteron beams was discussed recently (see [4] and references therein).

The theoretical estimation of antideuteron production preformed in the article in [1] are based on the well-known coalescence model [5] which supposes that two nucleons fuse into a deuteron if the momentum of their relative motion is smaller than a certain quantity p_0, the coalescence radius in momentum space. This momentum p_0 is considered as a free parameter to be fixed from the experimental data.

More than ten years ago, a quite simple diagrammatic approach to the coalescence model provided a microscopical basis for the coalescence model and expressed the parameter p_0 in terms of the slope parameter of the inclusive nucleon spectrum and the wave function of the produced nucleus [6]. Within this approach, it appears to be possible to explain the empirical fact of approximate equality of the values of the coalescence radii for the description of the yields of various light fragments under similar kinematical conditions.

The aims of this article are to generalize this diagrammatic approach to antinuclei production (by the introduction of threshold effects and by taking account of the anisotropy of the angular distributions) and to apply this model to the antideuteron production in proton-proton and proton-nucleus collisions. Particular attention will be paid to proton-proton collisions due to their interest for astrophysics. We will show that, in the cases where the inclusive antiproton production cross-section and deuteron wave function are well known, this approach can describe quite well the inclusive antideuteron production cross-section without any additional parameter.

Note that there are few articles in which the antideuteron production is discussed within different approaches [7–10]. Some of them require additional parameters to describe the experimental data and none of them describes the whole ensemble of experimental data.

The article is organized as follows. In sect. 2 the main ideas of the diagrammatic approach to the coalescence model are described and this approach is generalized to the case of antideuteron production. In sect. 3, the description of the experimental data is presented. Finally, we provide a brief summary of the results.

2 Diagrammatic approach to the coalescence model

Let us remind the reader the main ideas of the diagrammatic approach to the coalescence model [6]. As a basis for the coalescence model, the simplest Feynman dia-

[a] e-mail: duperray@isn.in2p3.fr
[b] e-mail: protasov@isn.in2p3.fr
[c] e-mail: avoronin@aha.ru

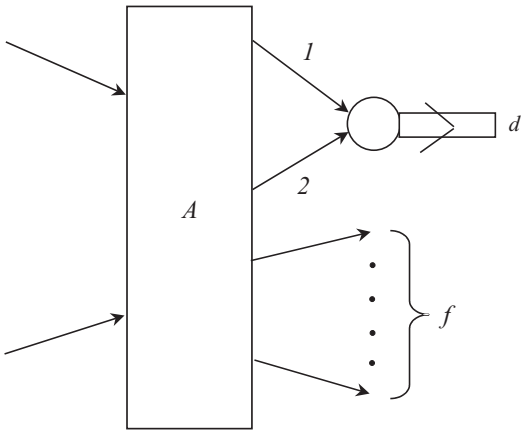

Fig. 1. The simplest Feynman diagram corresponding to coalescence of two nucleons into a deuteron.

gram of fig. 1, corresponding to the fusion of two nucleons is considered. Here the symbol f denotes the state of all other particles except the nucleons 1 and 2 which form the deuteron. The physical picture behind this diagram is quite simple: the nucleons produced in a collision (block A) are slightly virtual and can fuse without further interaction with the nuclear field. This simplest diagram is not the only possible contribution. However, as was shown in [11], there are mutual cancellations of a number of other diagrams and, as a result, the diagram of fig. 1 is the dominant one.

Let us remind briefly how to calculate this diagram by using the nonrelativistic technics developed in [12]. The amplitude M of this process can be written as

$$M = \int \frac{\mathrm{d}^3 p_1 \mathrm{d}E_1}{(2\pi)^4} \int \frac{\mathrm{d}^3 p_2 \mathrm{d}E_2}{(2\pi)^4} M_\mathrm{A} \times \frac{-2im_\mathrm{p}}{\mathbf{p}_1^2 - 2m_\mathrm{p}E_1 - i0} \frac{-2im_\mathrm{p}}{\mathbf{p}_2^2 - 2m_\mathrm{p}E_2 - i0} M_\mathrm{d} \times (2\pi)^4 \delta^3(\mathbf{p}_1 + \mathbf{p}_2 - \mathbf{P}) \delta(E_1 + E_2 - E - \varepsilon).$$

Here M_A is the diagram corresponding to the block A (production of nucleons 1 and 2 and other particles in the final state f), M_d the vertex of coalescence to the deuteron, m_p the nucleon mass. Two fractions are propagators of nucleons 1 and 2, the integrals are done over energies and momenta of these virtual particles. The last delta-functions reflect energy momentum conservation in the deuteron vertex ($\mathbf{P} = \mathbf{p}_1 + \mathbf{p}_2$ is the deuteron momentum, $E = \mathbf{P}^2/4m_\mathrm{p}$ its kinetic energy, $\varepsilon \approx -2.2$ MeV its binding energy).

After a trivial integration over $\mathbf{p}_2$ and E_2 and the introduction of the relative momentum $\mathbf{q} = \frac{1}{2}(\mathbf{p}_1 - \mathbf{p}_2)$, one obtains the following expression:

$$M = \int \frac{\mathrm{d}^3 q \mathrm{d}E_1}{(2\pi)^4} M_\mathrm{A}(\mathbf{P}, \mathbf{q}) M_\mathrm{d} \frac{-2im_\mathrm{p}}{(\mathbf{q} + \mathbf{P}/2)^2 - 2m_\mathrm{p}E_1 - i0} \times \frac{-2im_\mathrm{p}}{(\mathbf{q} - \mathbf{P}/2)^2 - 2m_\mathrm{p}(\mathbf{P}^2/4m_\mathrm{p} - E_1 + \varepsilon) - i0}.$$

The final integration over $\mathrm{d}E_1$ (one supposes as usually that the only singularities in the complex E_1-plane are those of propagators) gives

$$M = i \int \frac{\mathrm{d}^3 q}{(2\pi)^3} M_\mathrm{A}(\mathbf{P}, \mathbf{q}) \varphi_\mathrm{d}(\mathbf{q}), \quad (1)$$

where the deuteron wave function

$$\varphi_\mathrm{d}(\mathbf{q}) = \frac{m_\mathrm{p} M_\mathrm{d}}{\mathbf{q}^2 + m_\mathrm{p}|\varepsilon|}$$

is normalized by the condition

$$\int \frac{\mathrm{d}^3 q}{(2\pi)^3} |\varphi_\mathrm{d}(\mathbf{q})|^2 = 1.$$

To perform further calculations, one needs to make an assumption about the dependance of the amplitude M_A corresponding to the block A on its variables (the particle momenta). It can be shown [6], that the simplest hypothesis that this amplitude is constant gives rise to a wrong result: the production cross-section appears to be zero. One can see it from (1). When M_A does not depend on momenta the transition amplitude M becomes proportional to

$$M = iM_\mathrm{A} \int \frac{\mathrm{d}^3 q}{(2\pi)^3} \varphi_\mathrm{d}(\mathbf{q}) \propto \varphi_\mathrm{d}(\mathbf{r} = 0) = 0,$$

i.e. the deuteron wave function at the origin which, for realistic potentials, is equal to zero.

Therefore, the momentum dependence of M_A has to be introduced, for instance, in a "minimal" way: the inclusive nucleon spectra usually have a decreasing form and can be parameterized by a Gaussian function in rather wide parameter regions:

$$E_\mathrm{p} \frac{\mathrm{d}^3 \sigma_\mathrm{p}}{\mathrm{d}p_\mathrm{p}^3} \propto \exp\left(-\mathbf{p}_\mathrm{p}^2/Q^2\right), \quad (2)$$

where Q is related to the slope parameter. Accordingly, the amplitude M_A can be written in the following way:

$$M_\mathrm{A} = C \exp\left(-\frac{\mathbf{p}_1^2 + \mathbf{p}_2^2}{2Q^2}\right) = C \exp\left(-\frac{\mathbf{P}^2}{4Q^2} - \frac{\mathbf{q}^2}{Q^2}\right), \quad (3)$$

where the center-of-mass motion of the two nucleons is separated from their relative motion. The amplitude M_A determines the cross-section for the simultaneous production of two nucleons which can be expressed in a standard way which supposes a statistical independence in the production of the two nucleons as a product of inclusive cross-sections:

$$\frac{\mathrm{d}^6 \sigma_\mathrm{pn}}{\mathrm{d}p_\mathrm{p}^3 \mathrm{d}p_\mathrm{n}^3} = \frac{1}{\sigma_\mathrm{inel}} \frac{\mathrm{d}^3 \sigma_\mathrm{p}}{\mathrm{d}p_\mathrm{p}^3} \frac{\mathrm{d}^3 \sigma_\mathrm{n}}{\mathrm{d}p_\mathrm{n}^3}, \quad (4)$$

where σ_inel is the cross-section of the inelastic interaction of initial particles.

After the substitution of (3) into the expression for the diagram of fig. 1 and taking into account (4), the cross-section for the formation of deuterons takes the form

$$E_\mathrm{d} \frac{\mathrm{d}^3 \sigma_\mathrm{d}}{\mathrm{d}p_\mathrm{d}^3} = 12\pi^3 |S|^2 \frac{1}{m_\mathrm{p} \sigma_\mathrm{inel}} E_\mathrm{p} \frac{\mathrm{d}^3 \sigma_\mathrm{p}}{\mathrm{d}p_\mathrm{p}^3} E_\mathrm{n} \frac{\mathrm{d}^3 \sigma_\mathrm{n}}{\mathrm{d}p_\mathrm{n}^3}, \quad (5)$$

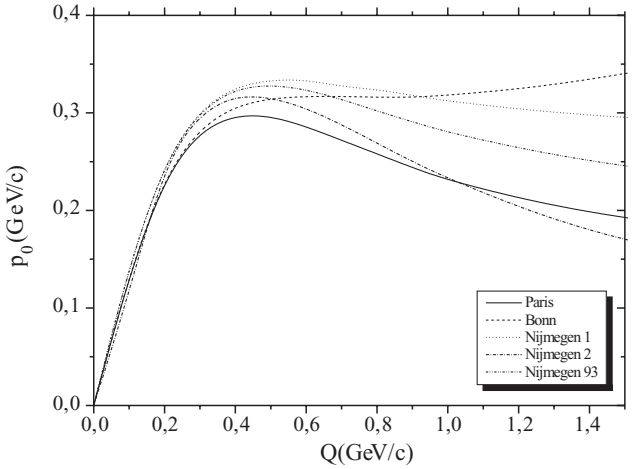

Fig. 2. Dependence of the coalescence momentum p_0 on the slope parameter Q of the inclusive nucleon spectrum for different nucleon-nucleon potentials.

where $\mathbf{p}_\mathrm{d} \approx 2\mathbf{p}_\mathrm{p}$, and

$$S = \int \frac{\mathrm{d}^3 q}{(2\pi)^3} \varphi_\mathrm{d}(\mathbf{q}) \exp\left(-\frac{\mathbf{q}^2}{Q^2}\right). \tag{6}$$

The structure of (4) is exactly the same as that of the coalescence model and one can obtain easily the following expression of the coalescence radius in momentum space[1]:

$$p_0^3 = 36\pi^2 \left| \int \frac{\mathrm{d}^3 q}{(2\pi)^3} \varphi_\mathrm{d}(\mathbf{q}) \exp\left(-\frac{\mathbf{q}^2}{Q^2}\right) \right|^2. \tag{7}$$

Thus, the approach based on the diagram of fig. 1 reproduces the coalescence model with p_0 which is no more a free parameter but it is determined by the inclusive proton spectrum and by the deuteron wave function. As an example, in fig. 2 the values of p_0 as a function of Q (eq. (8)) are presented for different nucleon-nucleon potentials (Paris [13], Bonn [14], and different versions of Nijmegen potential [15]).

One can see that all potentials give the same result up to $Q \approx 300$ MeV/c where the deuteron wave function in momentum space is quite well known. For higher values of Q the difference between the predictions of different nucleon-nucleon potentials can be very important (taking into account the fact that the cross-section is proportional to the third power of the coalescence radius in momentum space p_0). In this work, the Paris potential was chosen for further calculations.

The isotropic angular dependence supposed in (2) is quite frequently used in nonrelativistic collisions. In the relativistic case, the dependences on transversal and longitudinal momentum can be very different. However, the formulae obtained within this approach can be easily generalized to any angular dependence.

[1] In this definition of p_0, the spin of outgoing particles is not taken into account (see [6] for discussion). Note also that the definition of the parameter p_0 given in [1] differs from the standard one by a factor of 2.

If the inclusive nucleon cross-section is parameterized by an amplitude $M_{\mathbf{p}_1}$

$$E_1 \frac{\mathrm{d}^3\sigma_1}{\mathrm{d}p_1^3} = |M_{\mathbf{p}_1}|^2, \tag{8}$$

the cross-section for the deuteron formation can be written as (see (1))

$$E_\mathrm{d} \frac{\mathrm{d}^3\sigma_\mathrm{d}}{\mathrm{d}p_\mathrm{d}^3} = \frac{12\pi^3}{\sigma_\mathrm{inel} m_\mathrm{p}} \left| \int \frac{\mathrm{d}^3 q}{(2\pi)^3} M_{\mathbf{p}_1} M_{\mathbf{p}_2} \varphi_\mathrm{d}(\mathbf{q}) \right|^2. \tag{9}$$

It is clear that this model can be practically directly used to describe the production of antideuterons. The only problem is the presence of the threshold in the antiparticle production cross-sections. The coalescence model and the approach used here (10) are not valid in the near-threshold region. Therefore, one needs to propose a phenomenological procedure to describe experimental data near the threshold. For proton-proton collisions, the authors of [1] have proposed a quite simple prescription: the center-of-mass energy available for the production of the second antinucleon has to be reduced by twice the energy carried away by the first antinucleon $E_\bar{\mathrm{p}}$. In other words, the two antinucleons are supposed to be produced at different energies: $\sqrt{s}$ and $\sqrt{s} - 2E_\bar{\mathrm{p}}$.

In this article, the antideuteron production threshold is taken into account in a slightly different way. In proton-proton collisions, the main reaction giving antideuterons is $\mathrm{pp} \to \bar{\mathrm{d}}\mathrm{pppn}$. Near the threshold of this reaction, the energy dependence of the antideuteron production cross-section is mostly determined by the phase space of four nucleons $\Phi(\sqrt{s} - E_\bar{\mathrm{d}}; m, m, m, m)$,

$$E_\bar{\mathrm{d}} \frac{\mathrm{d}^3\sigma_\bar{\mathrm{d}}}{\mathrm{d}p_\bar{\mathrm{d}}^3} \propto \Phi(\sqrt{s} - E_\bar{\mathrm{d}}; m, m, m, m). \tag{10}$$

The phase space Φ for n-particles with masses, momenta and energies, respectively, m_i, $\mathbf{p}_i$, E_i is defined in the usual way (in cms):

$$\Phi(\sqrt{s}; m_1, m_2, \ldots m_n) = \prod_{i=1}^{n} \frac{1}{(2\pi)^3} \frac{\mathrm{d}^3 p_i}{2E_i} \delta^3\left(\sum_{i=1}^{n} \mathbf{p}_i\right) \delta\left(\sum_{i=1}^{n} \mathbf{E}_i - \sqrt{s}\right)$$

and is calculated by using the standard CERN library program [16]. $\sqrt{s}$ is the total energy available for these n-particles in the center-of-mass system.

Therefore, one can introduce a phenomenological correction factor R to the formula (10) defined as

$$R(\sqrt{s} - E_\bar{\mathrm{d}}) = \frac{\Phi(\sqrt{s} - E_\bar{\mathrm{d}}; m, m, m, m)}{\Phi(\sqrt{s} - E_\bar{\mathrm{d}}; 0, 0, 0, 0)}, \tag{11}$$

where the denominator contains the ultrarelativistic phase space to ensure R to be dimensionless and to have a correct behavior at high energies ($R \to 1$). The behavior of $R(x)$ is presented in fig. 3.

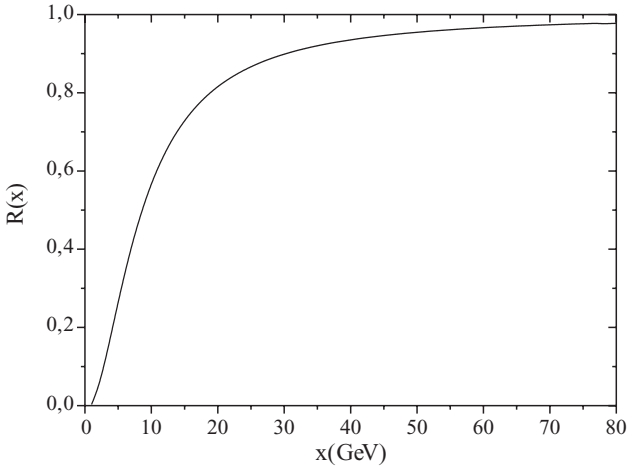

Fig. 3. Dependence of the threshold factor $R(x)$ on its argument.

There are, at least, two advantages with respect to the prescription chosen in [1]. Firstly, one makes no assumption about the mechanism of production. Secondly, this correction factor has a correct kinematic behavior both near the threshold and at high energies. We will discuss the role of this factor later.

3 Description of experimental data

Before presenting the results, let us make some preliminary remarks about the existing experimental data.

- The experimental data on antideuteron production are not abundant and are much less informative than those on deuteron production. There are only a few different experimental observations of antideuteron production in proton-proton [17–21], proton-nucleus [21–24], and nucleus-nucleus collisions [25–27]. Some experimental results cannot be analyzed within our approach because the experimental information is not complete. For instance, in [28] there is no data on antiproton production for corresponding energies; in [29] only relative spectra (antiprotons to π^- and antideuterons to π^-) were measured.
- To obtain a reasonable description within the present approach, one needs to know the cross-section of antiproton production for the antiproton momentum equal to a half of the antideuteron one. Unfortunately, this condition is rarely satisfied: in most experiments, the differential cross-sections of the antiproton and antideuteron production being measured for approximately the same momentum. Therefore, to apply the method one has to extrapolate the antiproton data to another kinematical region. This procedure, of course, introduces an additional error.
- In principle, the inclusive cross-sections discussed here are functions of two kinematical variables (for instance, transversal and longitudinal momentum) and one has to present the results in three-dimensional form. However, in each experiment one has only a few experimental points and the results are presented as a function of one variable (either total or transversal momentum).

The total inelastic cross-section was taken from the PDG data [30] (for proton-proton collisions) or described by the well-known parameterization [31] (for proton-nucleus and nucleus-nucleus collisions).

3.1 Proton-proton collisions

Let us begin the analysis with the most informative experiment performed on the ISR at CERN. In a few experiments, the spectra of antiprotons [32] and antideuterons [17,18] were measured in pp-collisions at $\sqrt{s} = 53$ GeV. The detector was situated at 90 degrees (in this geometry, the total momentum of outgoing particles coincides with the transversal one). Inclusive antiproton cross-sections over quite large regions of momentum and $\sqrt{s}$ were obtained in [32]. An example of an experimental distribution of antiprotons for $\sqrt{s} = 53$ GeV is presented in fig. 4 in comparison with two different parameterizations of the data.

The first parameterization (solid line) proposed by the authors of the experiment [32],

$$E_{\bar{\mathrm{p}}} \frac{\mathrm{d}^3\sigma_{\bar{\mathrm{p}}}}{\mathrm{d}p^3_{\bar{\mathrm{p}}}} = As^{\alpha} \exp[-Bp_{\mathrm{t}}], \tag{12}$$

with parameters $A = 0.195$ mbarn/(GeV/c)^2, $\alpha = 0.310$, $B = 2.49$ (GeV/c)$^{-1}$ describes perfectly these data. The second one (dashed line)

$$E_{\bar{\mathrm{p}}} \frac{\mathrm{d}^3\sigma_{\bar{\mathrm{p}}}}{\mathrm{d}p^3_{\bar{\mathrm{p}}}} = f \exp[-(Ap_{\mathrm{t}} + Bp^2_{\mathrm{t}})], \tag{13}$$

is the frequently used parameterization proposed by Tan and Ng [33] which works quite well in a wide region of

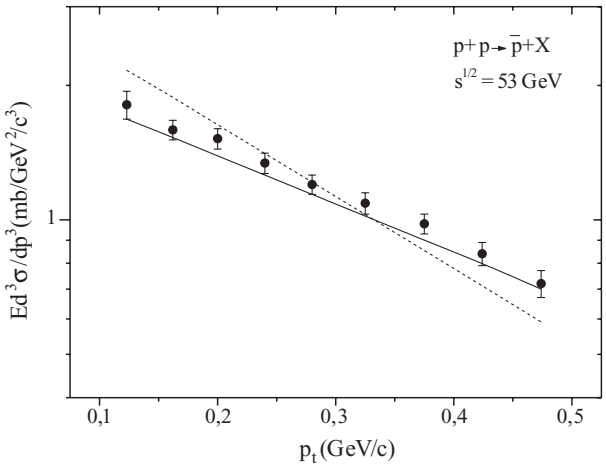

Fig. 4. The inclusive differential cross-section of antiproton production as a function of the transversal momentum p_{t} compared to two different parameterizations: solid line, exponential parametrization [32]; dashed line, Tan and Ng [33] parameterization. The data are taken from [32].

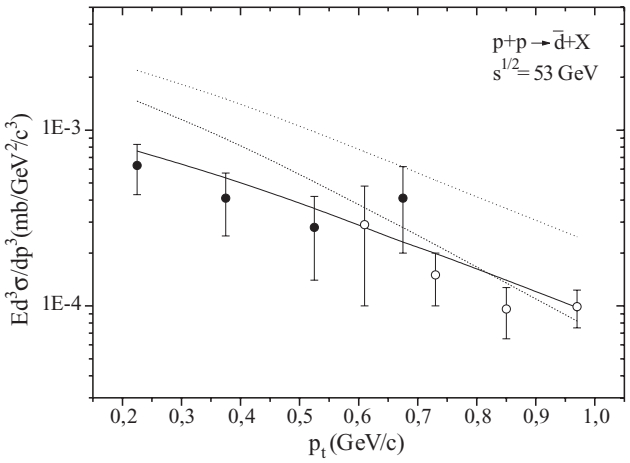

Fig. 5. The inclusive differential cross-section of antideuteron production as a function of the transversal momentum $p_{\rm t}$ compared to the calculations with two different parameterizations of the antiproton production cross-section: solid line, exponential fit; dashed line, Tan and Ng parameterization. The dotted line is the calculation with an exponential function without the anisotropy effect. The data are taken from [17] (black circles) and [18] (open circles).

$p_{\rm t}$ and $\sqrt{s}$. Here $f = f(E^*, \sqrt{s})$, $A = A(E^*, \sqrt{s})$ and $B = B(E^*, \sqrt{s})$ are known functions of $\sqrt{s}$ and of the antiproton energy in the center-of-mass system E^*. This formula gives here reasonable values of the cross-section but the trend is not well reproduced. We present here both quite close parameterizations to demonstrate the difference in description of the data on antideuteron production. The corresponding cross-section measured in this experiment [17,18] are given in fig. 5 and compared with different calculations.

Comparison between the two parameterizations shows that the description of the antideuteron production is quite sensitive to the antiproton production cross-sections: 20–30% difference in description of the $\bar{\rm p}$ data can result in a factor of 2 for the $\bar{\rm d}$. This difference can be even more pronounced if one has to extrapolate a chosen parameterization. As we mentioned previously $p_{\bar{\rm d}} \approx 2p_{\bar{\rm p}}$. This condition is satisfied for these ISR data. In some other experiments presented hereafter, it is not the case.

In this figure, one can see also the importance of the anisotropy of angular distributions. An exponential parameterization (13) of the antiproton production cross-section can be seen in two ways: as a function of the total antiproton momentum or of the transversal one (as stated previously, in the particular geometry of this experiment, they are equal to each other). However, in the integral (10), all directions (and not only transverse one) are presented and the difference between total and transversal momenta can be quite important. Thus, for the data under consideration the solid line represents the results with parameterization (13), whereas the dotted line corresponds to the same parameterization but with total momentum instead of the transversal one (antiproton production cross-section supposed to be isotropic).

By using the picture of the coalescence model, it is quite easy to see when anisotropy can be important in the description of the experimental data. If the total antideuteron momentum $p_{\rm cm}$ is very high with respect to the coalescence radius in momentum space p_0, antiproton and antineutron are produced in approximately the same direction (the direction of the antideuteron momentum) and the anisotropy of antinucleon angular distributions plays no role. If $p_0 \approx p_{\rm cm}$, the two antinucleons can propagate in quite different directions before coalescence and it is necessary to take anisotropy into account correctly.

For these ISR data, the total antideuteron momentum $p_{\rm cm}$ is of the order of the coalescence momentum p_0 and the anisotropy effect is seen clearly. In all other experimental data discussed hereafter, $p_{\rm cm}$ is very high with respect to p_0 and the anisotropy effect is not so important.

We can thus understand easily that if one uses anisotropic cross-sections the effect of the D-wave in the deuteron wave function can be quite important (for isotropic Gaussian parametrization (1), the D-wave contribution is explicitly equal to 0). For these ISR data, the introduction of the D-wave contribution into the deuteron wave function divides the value of the cross-section by a factor of 2.

In all calculations presented in this article, the Paris wave function is used. For most experimental data analyzed in this article, the choice of the deuteron wave function is not crucial: if the characteristic slope parameter of the inclusive antinucleon spectrum is less than approximately 0.5 GeV/c, all potential models give close values of p_0 (see fig. 2). However, for some sets of data it is not the case (we will mention them where necessary).

Another set of experimental data for the same $\sqrt{s}$ but with very large longitudinal component of antideuteron momentum $p_{\rm l} \approx$ 5–7 GeV/c was measured in [19] and is presented in fig. 6. The antiproton spectrum is taken

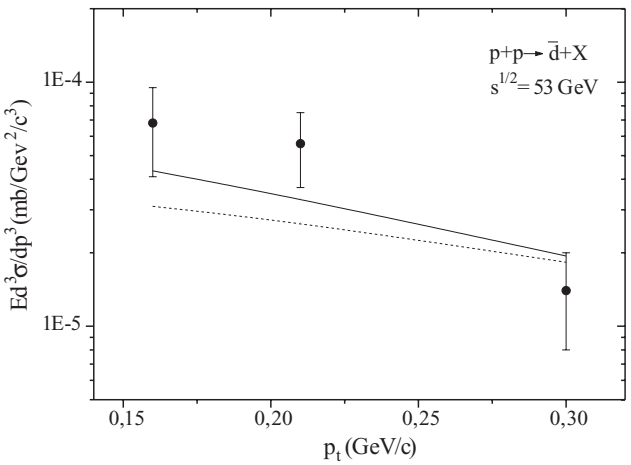

Fig. 6. The inclusive differential cross-section of antideuteron production as a function of the transversal momentum $p_{\rm t}$ compared to the calculations with two different parameterizations of the antiproton production cross-section: solid line, exponential function; dashed line, Gaussian. The data are taken from [19].

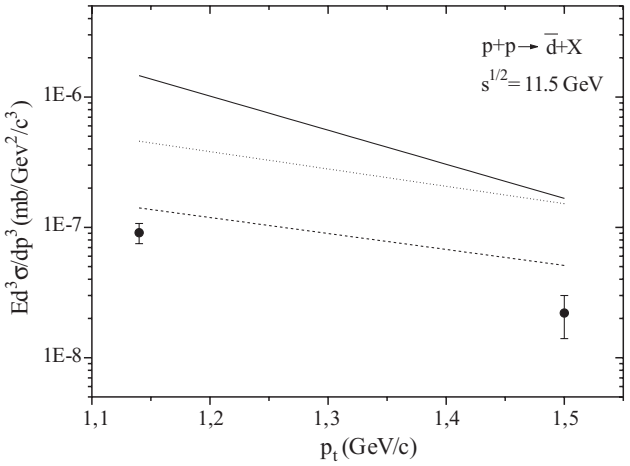

Fig. 7. The inclusive differential cross-section of antideuteron production as a function of the transversal momentum p_t compared to the calculations with two different parameterizations of the antiproton production cross-section: solid line, exponential function; dotted line, Gaussian. In both calculations, the threshold effect is not included. The third line (dashed) corresponds to calculations using the Gaussian parameterization including the threshold effect. The data are taken from [21].

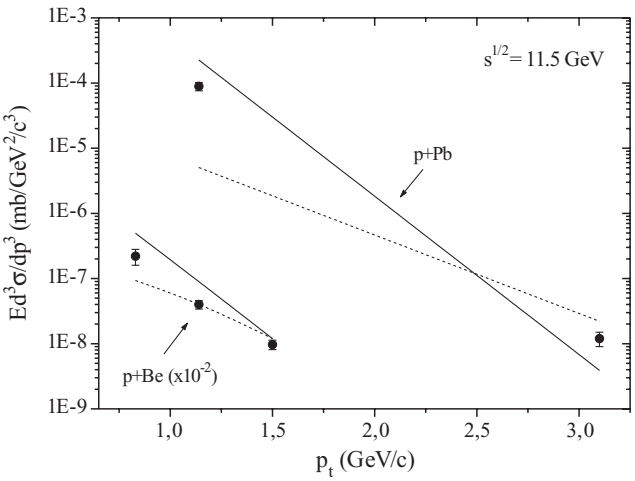

Fig. 8. The inclusive differential cross-section of antideuteron production on Be and Pb targets as a function of the transversal momentum p_t compared to the calculations with two different parameterizations of the antiproton production cross-section: solid line, exponential function; dashed line, Gaussian. The data are taken from [21].

from an experiment performed by this group [34]. Unfortunately, the parameterization of Tang and Ng does not work well here (its prediction exceeds systematically the data by a factor of 2). Therefore, we fitted the data by a Gaussian (proposed also by the authors of [34]) and by an exponential function of p_t. Both parameterizations give a quite good antideuteron production cross-section.

However, it appears to be impossible to reasonably describe another set of ISR data measured at very high momentum transfer [20]. The parameterization of Tang and Ng cannot reproduce the antiproton production cross-section: the order of magnitude is correct but its trend is not general which has a quite unusual form (the cross-section increases with increasing p_t! Thus, the absence of the $\bar{p}$ cross-section parameterization does not allow us to obtain a reasonable description of the $\bar{d}$ production data (the use of Tan and Ng parameterization as input gives a result 4–10 times higher than the experimental data).

The last measurement of $\bar{d}$ production in pp-collisions was performed ten years later at the IHEP machine [21] at lower cms energies ($\sqrt{s}$ = 11.5 GeV) and with different geometry (with fixed target). The data were taken at very high p_t and p_l and are not very rich (two points both for $\bar{p}$ and $\bar{d}$). Tang and Ng parameterization fails to describe the data (by a factor of ten for the highest momentum) and the characteristic slope parameter of the inclusive $\bar{p}$ spectrum is quite high (where different potential models give quite different (by a factor of 2) predictions). However, we decided to present this instructive example because one can estimate here the role of the threshold effect by the procedure proposed in (12). One can fit the antiproton data (two points) both by a Gaussian and an exponential function of p_t. The corresponding predictions for the $\bar{d}$ production cross-section are given in fig. 7 by the dotted and solid line, respectively (without threshold effect). Once the threshold is taken into account by the introduction of the factor R (12), the agreement with the experimental data is improved significantly (the dashed line represents the calculations with an exponential parameterization and the threshold effect).

3.2 Proton-nucleus collisions

Unfortunately, there are no more exploitable data on the antideuteron production in proton-proton collisions. To test further the model, we analyzed the available data on the $\bar{d}$ production in proton-nucleus collisions. Here, one has no more general parameterization like [33] and, for each set of data, a different parameterization is used[2].

In the same IHEP experiment [21], the production of antideuterons was measured on Be and Pb targets also.

For these data, one can make the same remarks as for the data obtained in the proton-proton collisions (only a few experimental points, very high momenta of outgoing particles, and quite high value of the slope parameter). The results are presented in fig. 8 and look quite encouraging.

There are also old IHEP measurements of the antideuteron production in p-Al collisions [22,23]. The data were taken in the forward (or practically forward) direction and we have no information about the p_t-dependence of the antiproton production cross-section (thus we cannot take completely into account the anisotropy of angular distributions). Therefore, in fig. 9, the results of the calculations and the data are presented as a function of the

[2] Note that in high-energy proton-nucleus and nucleus-nucleus collisions, the physical center-of-mass system is the nucleon (from the target) - nucleon (from the beam) one.

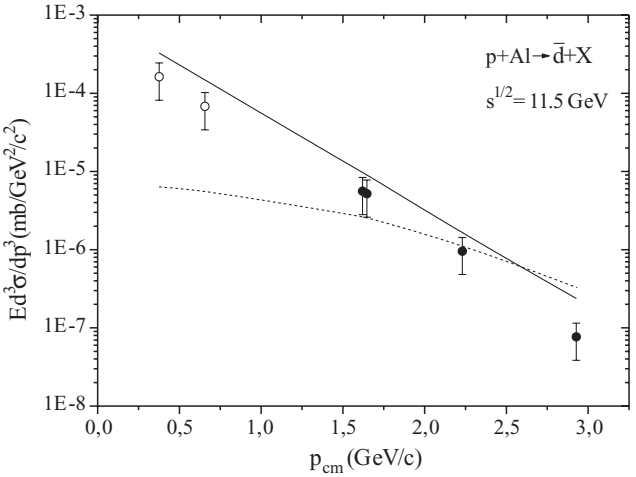

Fig. 9. The inclusive differential cross-section of antideuteron production on Al target as a function of the total momentum in the center-of mass frame compared to the calculations with two different parameterizations of the antiproton production cross-section: solid line, exponential function; dashed line, Gaussian. The data are taken from [22] (black circles) and [23] (open circles).

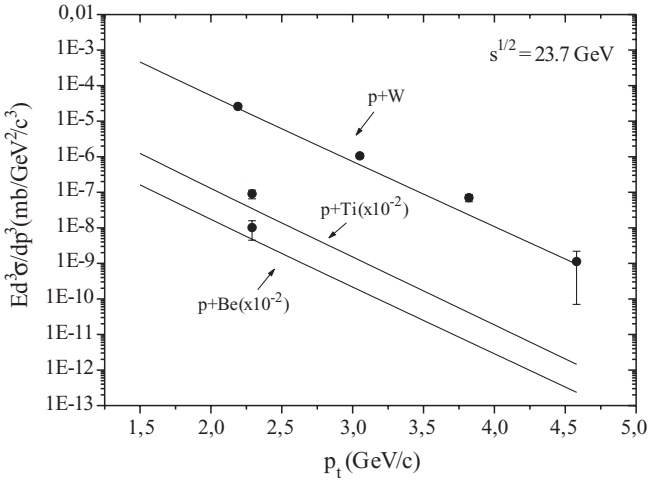

Fig. 10. The inclusive differential cross-section of antideuteron production on Be, Ti, and W targets as a function of the transversal momentum p_{t} compared to the calculations with exponential parameterization of the antiproton production cross-section. The data are taken from [24].

total $\bar{\mathrm{d}}$ momentum. Note that, for the Gaussian function, the value of the slope parameter Q appears to be very large (of the order of 1.3 GeV/c), where the deuteron wave function is not known and the results depend strongly on the nuclear potential.

This analysis can be completed by the measurement performed in FNAL [24], where the antideuteron production cross-section was measured for different targets (Be, Ti, W) at intermediate (with respect to the ISR and IHEP experiments) energies ($\sqrt{s} = 23.7$ GeV/c). The data were taken at quite high transverse momentum. The theoretical results presented in fig. 10 are in quite good agreement with the experimental data for the three targets. One of the reasons for this good agreement is a good knowledge of the antiproton production cross-section obtained in this experiment.

It is necessary to note that there are also some experimental results on antideuteron production in nucleus-nucleus collision obtained in the AGS experiment (one point in Si + Al collision [25] and two points in Au + Pb [26]) and in the NA52 experiment [27]. Unfortunately here, one has neither a good parameterization of the antiproton production cross-section nor a reliable parameterization for the total inelastic cross-section. The measurements were made in the forward direction and one has no information about the p_{t}-dependance of the antiproton production cross-sections (thus, it is impossible to take into account correctly the anisotropy of angular distributions which can be very important here). Simple parameterizations (Gaussian and exponential) gave no satisfactory description. In general, the discrepancy between the calculations and the data is of the order of a factor 5, which is not very surprising taking into account all these remarks. As an example, in fig. 11 the calculation of the antideuteron production cross-section

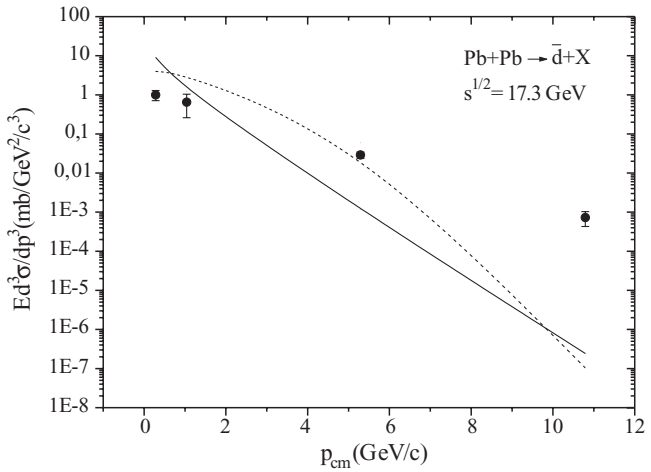

Fig. 11. The inclusive differential cross-section of antideuteron production in Pb-Pb collisions as a function of total momentum in the center-of-mass frame compared to the calculations with two different parameterizations of the antiproton production cross-section: solid line, exponential function; dashed line, Gaussian. The data are taken from [27].

in Pb + Pb collisions as a function of total momentum in the center-of-mass frame in comparison with the experimental data [27] is presented. The data cover a very large momentum region and the characteristic momentum in the antiproton production cross-section is very high (of the order of 2 GeV/c).

4 Conclusions

Our main conclusion is that the diagrammatic approach to the coalescence model developed in [6] can be successfully applied to the description of the antideuteron production

in proton-proton and proton-nucleus collisions. There are two modifications: firstly, it is necessary to take into account the threshold effect and, secondly, one must include specific consideration of the strong anisotropy of the angular distributions of antiproton production. Once these phenomena are taken into account, the model can describe most of the existing experimental data on the antideuteron production in proton-proton and proton-nucleus collisions.

The successful reproduction of experimental data suggests that a good knowledge of the antinucleon production cross-section and of the deuteron wave function allow to describe the antideuteron production cross-section in a quite large region of kinematic variables without any additional parameter.

During the preparation of this article, we learnt about the death of our friend and colleague V.M. Kolybasov who proposed the model discussed in this article. We would like to dedicate this work to his memory. The authors would like to thank A. Barrau, M. Buénerd, A.J. Cole, L. Dérome, V.A. Karmanov and P. Salati for very useful and stimulating discussions.

References

1. P. Chardonnet, J. Orloff, P. Salati, Phys. Lett. B **409**, 313 (1997).
2. S. Ahlen *et al.*, Nucl. Instrum. Methods A **350**, 351 (1994).
3. O. Adrani *et al.*, Nucl. Instrum. Methods A **478**, 114 (2002).
4. F. Iazzi, Nucl. Phys. A **655**, 371c (1999).
5. S.T. Butler, C.A. Pearson, Phys. Rev. Lett. **7**, 69 (1961); Phys. Lett. **1**, 77 (1962); Phys. Rev. **129**, 836 (1963); A. Schwarzschild, C. Zupancic, Phys. Rev. **129**, 854 (1963); L.P. Csernai, J.I. Kapusta, Phys. Rep. **131**, 223 (1985).
6. V.M. Kolybasov, Yu.N. Sokol'skikh, Phys. Lett. B **225**, 31 (1989); Sov. J. Nucl. Phys. **55**, 1148 (1992).
7. S. Mrówczyński, Phys. Lett. B **248**, 459 (1990).
8. C.B. Dover, U. Heinz, E. Schneidermann, J. Zimányi, Phys. Rev. C **44**, 1636 (1991).
9. S. Leupold, U. Heinz, Phys. Rev. C **59**, 1110 (1994).
10. R. Scheibl, U. Heinz, Phys. Rev. C **59**, 1585 (1999).
11. M.A. Braun, V.V. Vechernin, Sov. J. Nucl. Phys. **44**, 506 (1986); **36**, 357 (1982).
12. I.S. Shapiro, *Dispersion Theory of direct nuclear reactions*, in *Selected Topics in Nuclear Theory*, edited by F. Janouch (IAEA, Vienna, 1963); I.S. Shapiro, Usp. Fiz. Nauk. **92**, 549 (1967) (Sov. Phys. Usp. **10**, 515 (1968)).
13. M. Lacombe, B. Loiseau, R. Vinh Mau, J. Côté, P. Pirés, R. de Toureil, Phys. Lett. B **101**, 139 (1981).
14. R. Machleidt, K. Holinde, Ch. Elster, Phys. Rep. **149**, 1 (1987).
15. V.G. Stoks, *et al.*, Phys. Rev. C **49**, 2950 (1994); `http://nn-online.sci.kun.nl/`.
16. F. James, Monte Carlo Phase Space, CERN 68-15 (1968); `http://wwwinfo.cern.ch/asdoc/shortwrupsdir/w515/top.html`.
17. B. Alper *et al.*, Phys. Lett. B **46**, 265 (1973).
18. W.M. Gibson *et al.*, Lett. Nuovo Cimento **21**, 189 (1978).
19. M.G. Albrow *et al.*, Nucl. Phys. B **97**, 189 (1975).
20. J.C.M. Armitage *et al.*, Nucl. Phys. B **150**, 87 (1979).
21. V.V. Abramov *et al.*, Sov. J. Nucl. Phys. **45**, 845 (1987).
22. F. Binon *et al.*, Phys. Lett. B **30**, 510 (1969).
23. Yu.M. Antipov *et al.*, Phys. Lett. B **34**, 164 (1969).
24. J.W. Cronin *et al.*, Phys. Rev. D **11**, 3105 (1975).
25. A. Aoki *et al.*, Phys. Rev. Lett. **69**, 2345 (1992).
26. T.A. Armstrong *et al.*, Phys. Rev. C **59**, 2699 (1999).
27. G. Appelquist *et al.*, Phys. Lett. B **376**, 245 (1996).
28. D.E. Dorfan *et al.*, Phys. Rev. Lett. **14**, 1003 (1992).
29. W. Bozzoli *et al.*, Nucl. Phys. B **144**, 317 (1978).
30. PDG, Review of Particle Physics, Eur. Phys. J. C **15**, 1 (2000); `http://pdg.web.cern.ch/pdg/`.
31. J. Javos *et al.*, Phys. Rev. C **18**, 2273 (1978).
32. K. Guettler *et al.*, Nucl. Phys. B **116**, 77 (1976).
33. L.C. Tang, L.K. Ng, Phys. Rev. D **26**, 1179 (1982).
34. M.G. Albrow *et al.*, Phys. Lett. B **42**, 279 (1972).